Since January 2020 Elsevier has created a COVID-19 resource centre with free information in English and Mandarin on the novel coronavirus COVID-19. The COVID-19 resource centre is hosted on Elsevier Connect, the company's public news and information website.

Available online at www.sciencedirect.com
ScienceDirect
Virus Research 132 (2008) 76–85
Virus Research
www.elsevier.com/locate/virusres

Cytoplasmic vacuolization responses to cytopathic bovine viral diarrhoea virus

Alexander V. Birk [a,c,*], Edward J. Dubovi [b], Leona Cohen-Gould [a], Ruben Donis [d], Hazel. H. Szeto [a]

[a] *Department of Pharmacology, Weill Medical College of Cornell University, New York, NY 10021, United States*
[b] *Department of Population Medicine and Diagnostic Science, College of Veterinary Medicine, Cornell University, Ithaca, NY 14853, United States*
[c] *Institute of Hepatitis and Viral Research, 3805 Old Easton Road, Doylestown, PA 18902, United States*
[d] *Influenza Branch, Division of Viral & Rickettsial Diseases Centers for Disease Control and Prevention, 1600 Clifton Road-Mail Stop G-16, Atlanta, GA 30333, United States*

Received 23 August 2007; received in revised form 17 October 2007; accepted 19 October 2007
Available online 3 December 2007

Abstract

Bovine Viral Diarrhea Virus (BVDV) is a positive sense, single-stranded RNA virus which exhibits two biotypes in standard cell culture systems. The cytopathic strains of this virus (cpBVDV) induce dramatic cytoplasmic vacuolization in cell cultures, while infection with the non-cytopathic (NCP-BVDV) strains produces no overt changes in the host cells. Our results show that extensive cytoplasmic vacuolization is the earliest morphological change in response to cpBVDV infection in MDBK cells. Cells with extensive vacuolization showed no co-existing chromatin condensation, caspase activation, or loss of membrane integrity. In addition, the caspase inhibitor (zVAD-fmk), although improving cell viability of infected cells from $6.7 \pm 2.2\%$ to $18.8 \pm 2.2\%$, did not prevent vacuolization. On the ultrastructural level, the virus-induced cytoplasmic vacuoles are single membrane structures containing organelles and cellular debris, which appear capable of fusing with other vacuoles and engulfing surrounding cytoplasmic materials. LysoTracker Red which marks lysosomes did not stain the virus-induced cytoplasmic vacuoles. In addition, this lysosomal dye could be observed in the cytoplasm of vacuolized cells, suggesting a lysosomal abnormality. Our data demonstrate that cpBVDV induced a novel cell death pathway in MDBK cells that is primarily associated with lysosomal dysfunction and the formation of phagocytic cytoplasmic vacuoles, and this mode of cell death is different from apoptosis and necrosis.

Keywords: RNA virus; BVDV; Vacuolization; Cell death; Cellular response

1. Introduction

Bovine Viral Diarrhea Virus (BVDV) is a positive sense, single-stranded RNA virus that belongs to the Flaviviridae family (Collett et al., 1988). BVDV is known to cause severe lesions in the gastrointestinal tract and death in affected animals (Bolin et al., 1985; Brownlie et al., 1984). Two biotypes, cytopathic (cpBVDV) and noncytopathic (ncpBVDV), can be isolated from infected animals exhibiting the classical mucosal disease syndrome (Brownlie, 1991). However, only cpBVDV induces cytopathology in sensitive cell types, such as Madin-Darby bovine kidney cells (MDBK).

cpBVDV induces dramatic cytoplasmic vacuolization in infected cell cultures and in tissues of infected calves (Bielefeldt Ohmann and Bloch, 1982), commonly referred to as cytopathic effects (CPE) of cpBVDV. To date, the nature of this vacuolization during BVDV infection is not understood. Recently, it was suggested that cpBVDV-induced apoptosis is responsible for the virus-associated CPE (Grummer et al., 1998; Zhang et al., 1996). However, the morphology of apoptotic cell death is generally not associated with cytoplasmic vacuoles. Furthermore, although inhibitors of apoptosis, including zVAD-fmk, blocked apoptosis in cpBVDV-infected cells and significantly improved cell survival, they failed to achieve suppression of cytoplasmic vacuolization (Bendfeldt et al., 2003; Grummer et al., 2002a).

* Corresponding author at: Institute of Hepatitis and Viral Research, 3805 Old Easton Road, Doylestown, PA 18902, United States. Tel.: +1 215 489 4900; fax: +1 215 489 4920.
E-mail address: avbirk@ihvr.org (A.V. Birk).

0168-1702/$ – see front matter © 2007 Elsevier B.V. All rights reserved.
doi:10.1016/j.virusres.2007.10.017

In this paper we report that cpBVDV-induced rapid and extensive vacuolization in MDBK cells, which is morphologically different from apoptosis and necrosis. This cellular response was characterized by electron microscopy, which shows the presence of enlarged single membrane vacuoles containing organelles and cellular debris, capable of fusing with other vacuoles and engulfing surrounding cytoplasmic materials.

2. Experimental procedures

2.1. Chemicals

All cell culture supplies and fluorescent probes were obtained from Invitrogen (Carlsbad, CA). Unless specified, all other reagents were supplied by Sigma–Aldrich (St. Louis, MO).

2.2. Cells and viruses

MDBK cells (ATCC-CCL22) or fetal bovine kidney cells (FBK) derived from primary tissue, were grown in Dulbecco's Modified Eagle's Minimum Essential Medium (DMEM) containing 4.5 g of glucose, and 10% horse serum in cell culture incubator (5% CO_2, 37 °C). Cells were infected with plaque-purified cpBVDV strain NADL in cell culture medium, the ncpBVDV strain NY-1 or mock-infected with cell culture medium alone. The titer of BVDV used in our studies was sufficient to generate an input MOI of 3–5 which can completely destroy MDBK cell monolayers and kill 90% of cells within 72 h of infection or for ncpNY-1 produce a positive fluorescent stain in 100% of the infected cells.

After initial incubation for 1 h in cell a culture incubator (5% CO_2, 37 °C), the culture medium was changed to a fresh virus-free medium. For some experiments, either wortmannin (PI3-kinase inhibitor) or zVAD-fmk (pan-caspase inhibitor) was added in required final concentration and then incubated for the next 48 or 72 h. zVAD-fmk was replenished every 10–12 h as suggested in the literature (Bendfeldt et al., 2003). Cells were then further incubated for an intended duration of time in the presence or absence of the inhibitor.

2.3. Cell viability

MDBK cells were plated at a density 1–2 × 10^3 cells/well in 96 well plates. On the following day, after initial infection for 1 h, cells were washed and medium containing required inhibitors were added to cells and incubated for needed period of time. Then, cell viability was assessed using the Resaruzin (Almar blue) indicator dye (Mazzio and Soliman, 2004). Quantitative analysis of dye conversion was measured using a fluorescent plate reader with ex/em = 550/580. Cell viability was expressed as percentage of untreated cells.

2.4. Light and fluorescent microscopy

2.4.1. Detection of cytoplasmic vacuolization

Mock-infected, cpBVDV-infected, and NY-1 infected MDBK cells were grown on 96- or 24-well plates in defined medium for 6, 16, or 24 h post-infection. At these time points cells were subjected to the light microscopy using a Zeiss fluorescent microscope and photographed. All images were processed and analyzed by counting total number of cells and number of vacuolized cells. Very often those cells were also examined for signs of apoptosis including chromatin condensation (Hoechst 33342) and caspase activation (FLICA (*for details, see below*). This allowed us to superimpose light and fluorescent microscopic images to determine if vacuolization and characteristics of apoptosis co-exist in the same cell. All experiments were done in triplicates and each "*n*" represents 3–6 fields from each of three different wells for each time point (6, 16, and 24 h post-infection) in the presence or absence of cpBVDV.

2.4.2. Detection and cellular localization of viral NS3 in MDBK cells

To determine cellular localization of the nonstructural BVDV protein NS3 while preserving cellular architecture infected or control cells were fixed in 0.1% gluteraldehyde for 10 min. Cells were then incubated in 1% Triton ×100 for 30 min, washed in PBS, and stained for NS3 using BVDV Mab 20.1.6 according to published methodology (Deregt et al., 2005).

2.4.3. Detection of apoptosis by Hoechst staining

MDBK cells were grown on 96-or 24-well plates. Cells were then stained with 1 μg/ml Hoechst 33342 for 20 min, washed with cell culture medium, and imaged using a Zeiss fluorescent microscope equipped with a camera. Nuclear morphology was evaluated using an excitation wavelength of 350 ± 10 nm and a longpass filter of 400 nm for emission. All images were processed and analyzed by counting total number of cells, vacuolized cells and cells with apoptotic nuclei. Uniformly stained nuclei were scored as healthy, viable cells, while condensed or fragmented nuclei were scored as apoptotic. All experiments were done in triplicate and each "*n*" represents 3–6 fields from 3 different wells for each time point (6, 16, and 24 h post-infection) in the presence or absence of cpBVDV.

2.4.4. Detection of apoptosis by FLICA staining

Mock-infected and cpBVDV-infected MDBK cells were grown on 96-or 24-well plates for 24 h post-infection were assayed for the caspase activity using a commercial kit based on fluorochrome-labeled caspase inhibitors (FLICA, Immunochemistry Technologies LLC, Bloomington, MN), according to manufacturer's instructions. Cells were imaged by fluorescence microscopy (ex/em = 488/520 nm) and the images were processed and analyzed by counting total number of cells, vacuolized cells and FLICA-stained cells. All experiments were done in triplicate and each "*n*" represents 3–6 fields from 3 different wells.

2.4.5. Detection of necrosis by propidium-iodide staining

Propidium iodide (2.5 μg/ml) (Immunochemistry Technologies LLC, Bloomington, MN) was incubated with infected MDBK cells and nuclear localization was determined using a Zeiss fluorescent microscope as described above. Cellular morphology was evaluated using ex/em wavelengths of 552/570 nm.

All images were processed and light and fluorescent microscopy images were superimposed to determine propidium-iodide staining in highly vacuolized cells.

2.4.6. Detection of lysosomes by LysoTracker Red staining

MDBK cells were grown on 24-well plates. All treatments were carried out in quadruplicates. Cells were then stained with 100 nM LysoTracker Red for 20 min, washed in cell culture medium, and imaged using a Zeiss fluorescent microscope as described above. Cellular morphology was evaluated using ex/em wavelengths of 552/570 nm. All images were processed and light and fluorescent microscopy images were superimposed to determine lysosomal staining in highly vacuolized cells.

2.5. Electron microscopy

Cells were grown in 6-well plates for 24 h prior to infection with cpBVDV. Sixteen hours post-infection cells were washed with serum-free medium and fixed with fixation buffer (2.5% glutaraldehyde, 4% paraformaldehyde, 0.02% picric acid in 0.1 M buffer) for 60 min and then washed with the same buffer. Post-fixation was done in 1% OsO_4-1.5% K-ferricyanide (aqueous) for 60 min and then washed. After staining with 1.5% uranyl acetate for 30 min, dehydration was done through graded ethanol series. Samples were then infiltrated and embedded in LX-112 resin (Ladd Research Industries, Burlington, VT) by inserting tubes made from BEEM capsules into the resin prior to polymerization. Sections were cut at 55–60 nm (silver–gold) using a Diatome diamond knife (Diatome, USA, Hatfield, PA) on an RMC MT-7000 Ultramicrotome. (Boeckeler-RMC Instruments, Tucson, AZ). Sections were then contrasted with lead citrate and viewed on a JSM 100 CX-II electron microscope (JEOL, USA, Inc., Peabody, MA) operated at 80 kV. Images were recorded on Kodak 4489 Electron Image film then digitized on an Epson Expression 1600 Pro scanner at 900 dpi.

3. Results

The morphology of MDBK cells infected with cpBVDV (NADL) was practically indistinguishable from mock-infected control cells up to 6 h post-infection. However, by 16 and 24 h after infection, about 15 and 25% of total number of cells, respectively, were found to have extensive vacuolization of cytoplasm (Fig. 1A and B). In addition, by 24 h post-infection, vacuolized cells started to round up and detach, suggesting that virus-induced dynamic cellular pathology in whole population of cells have to be investigated within first 24 h. By 24–36 h post-infection, about 50% of monolayers in all wells inspected for this study were partially destroyed. Further incubation of infected cells beyond 36 h post-infection resulted in a significant number of detached cells, making it difficult to determine the mode of the cell death. Infection of MDBK cells with the noncytopathic strain of BVDV (NY-1) did not result in cytoplasmic vacuolization or disruption of the cellular monolayer (Fig. 1A). In addition, ncpBVDV-infected MDBK cells could be easily cultured without any morphological signs of infection. Infection of FBK cells with NADL also resulted in appearance

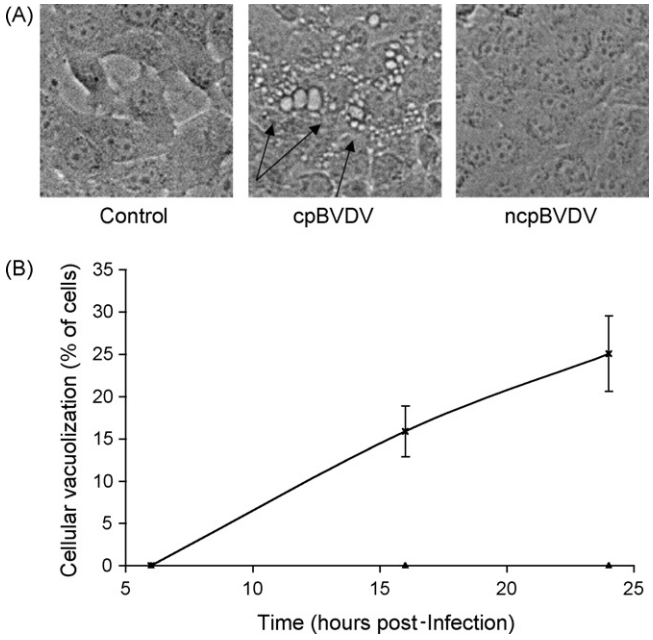

Fig. 1. cpBVDV infection induces cytoplasmic vacuolization in MDBK cells in a time-dependent manner. (A) Microscopic analysis of a representative control, cpBVDV, and ncpBVDV-infected MDBK cells at 24 h post-infection. Arrows indicate representative vacuolized cells in slides 24 h post-infection. (B) Vacuolized cells in mock-infected (▲) and cpBVDV-infected (*) samples were analyzed and counted as described in Section 2. Error bars indicate standard deviation for each time point and specified condition ($n = 3$).

of vacuolized cells, which were not observed in uninfected cells (data not shown).

Infection of MDBK cells with cpBVDV was confirmed by immunohistochemistry using a monoclonal antibody to viral NS3 protein 24 h post-infection (Fig. 2, right panel). Cells which stained for the viral protein also showed extensive cytoplasmic vacuolization. NS3 staining was observed throughout the cytoplasm, but the nucleus and cytoplasmic vacuoles were unstained. Uninfected cells were always NS3 negative (Fig. 2, left panel). These data clearly show that the vacuolated cells were not simply responding to being next to an infected cell.

To demonstrate that virus-induced cytoplasmic vacuoles were not due to degeneration of plasma membrane and necrosis, we stained MDBK cells with propidium iodide (PI) at 24 h post-infection. No PI staining was observed in any cells, including those with a large number of cytoplasmic vacuoles (indicated by arrows) (Fig. 3A). In control experiments, treatment of the same cells with 0.1 mM of diethyl pyrocarbonate (DEPC) (0.1 mM) for 10 min to permeabilize the cell plasma membrane resulted in a rapid uptake of PI into cells as evidenced by the stained nuclei (Fig. 3B). In addition, on the ultrastructural level, abnormal and swollen mitochondria, which are commonly found during necrosis and necroptosis (Degterev et al., 2005), were not detected in infected cells with extensive cytoplasmic vacuolization (Figs. 6B and 7).

Because previous studies have reported cpBVDV-induced apoptotic cell death (Grummer et al., 1998, 2002a; Jordan et al., 2002; Yamane et al., 2005), we compared the proportion of cells expressing characteristics of apoptosis, such as chromatin

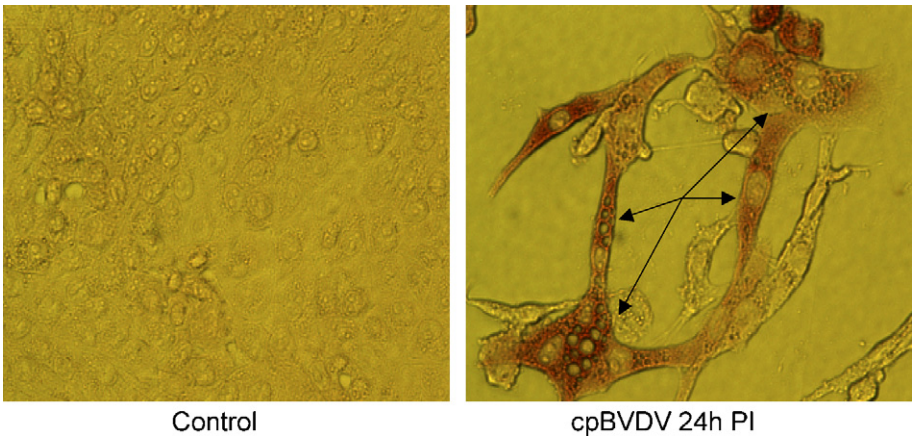

Fig. 2. Cytoplasmic vacuolization in MDBK cells expressing NS3 viral protein. Microscopic analysis of a representative control and cpBVDV-infected MDBK cells at 24 h post-infection, stained for NS3 viral protein. Arrows indicate representative vacuolized cells in slides 24 h post-infection.

condensation and caspase activation, with those undergoing extensive cytoplasmic vacuolization. A hallmark of apoptosis, chromatin condensation, can be observed using the Hoechst 33824 reagent, which brightly stains condensed chromatin. Chromatin condensation was determined to be in only $4 \pm 0.9\%$ of cells at 24 h post-infection (Fig. 4) whereas vacuolization was >25%. Caspase activation, quantified using Flica staining, was detected in only $15.3 \pm 1.7\%$ of all cells at 24 h post-infection (Fig. 4).

To determine the involvement of caspase activation in cpBVDV-induced cytoplasmic vacuolization, we used the general caspase inhibitor, zVAD-fmk (100 μM), which was shown to inhibit apoptosis in BVDV-infected cells (Bendfeldt et al., 2003). We found that, although addition of 100 μM zVAD-fmk

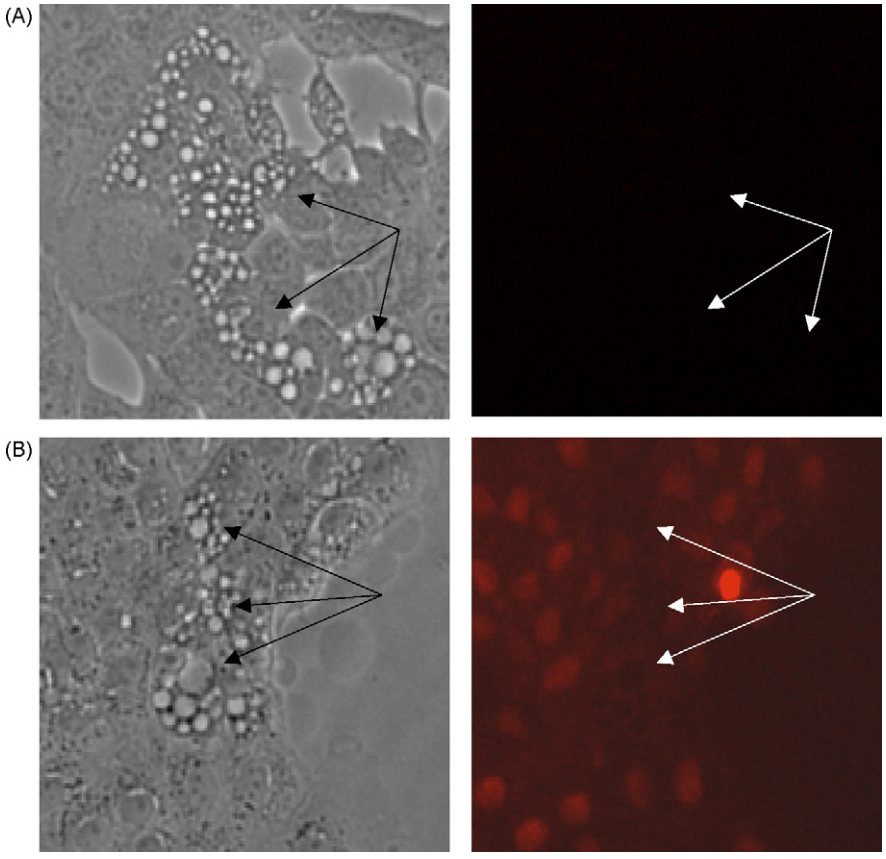

Fig. 3. cpBVDV-induced cytoplasmic vacuolization is not associated with loss of plasma membrane integrity. (A) Infected cells (24 h post-infection) were stained with propidium iodide (PI) and analyzed using fluorescent microscopy. Vacuolated areas (arrows) show no sign of PI localization in nuclei. (B) Infected cells (24 h post-infection) were treated with 0.1 mM DEPC for 10 min and stained with propidium iodide and analyzed using fluorescent microscopy, as described in Section 2. Arrows indicated vacuolated cells.

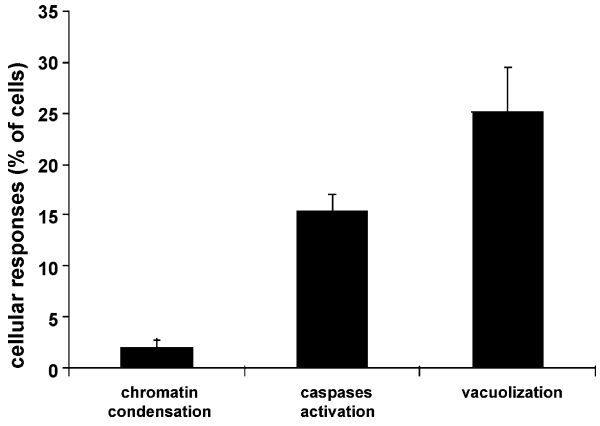

Fig. 4. Cytoplasmic vacuolization and apoptotic responses in cpBVDV-infected MDBK cells. Control and cpBVDV-infected cells were stained with Hoechst and FLICA dyes, for chromatin condensation and caspases activation, respectively, at 24 h post-infection. Vacuolized and dye-stained cells, were then analyzed and counted. Error bars indicate standard deviation for each specified analysis ($n = 3$).

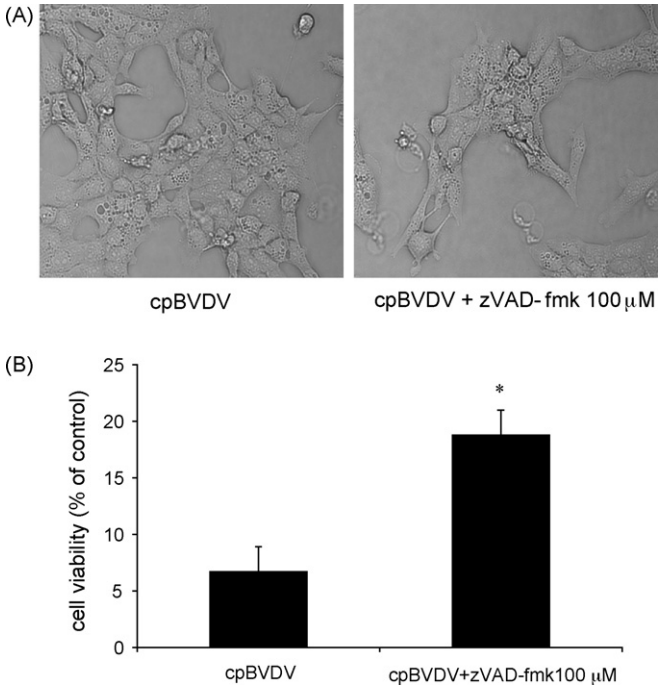

Fig. 5. Inhibition of caspase activation in infected cells partially prevents cpBVDV-induced cell death but does not block cytoplasmic vacuolization. (A) Light microscopy of infected MDBK cell (16 h post-infection) demonstrates that cpBVDV-induced cytoplasmic vacuolization is not affected by treatment with 100 μM zVAD-fmk. (B) Effect of zVAD-fmk (100 μM) on cell viability in cpBVDV infected cells.

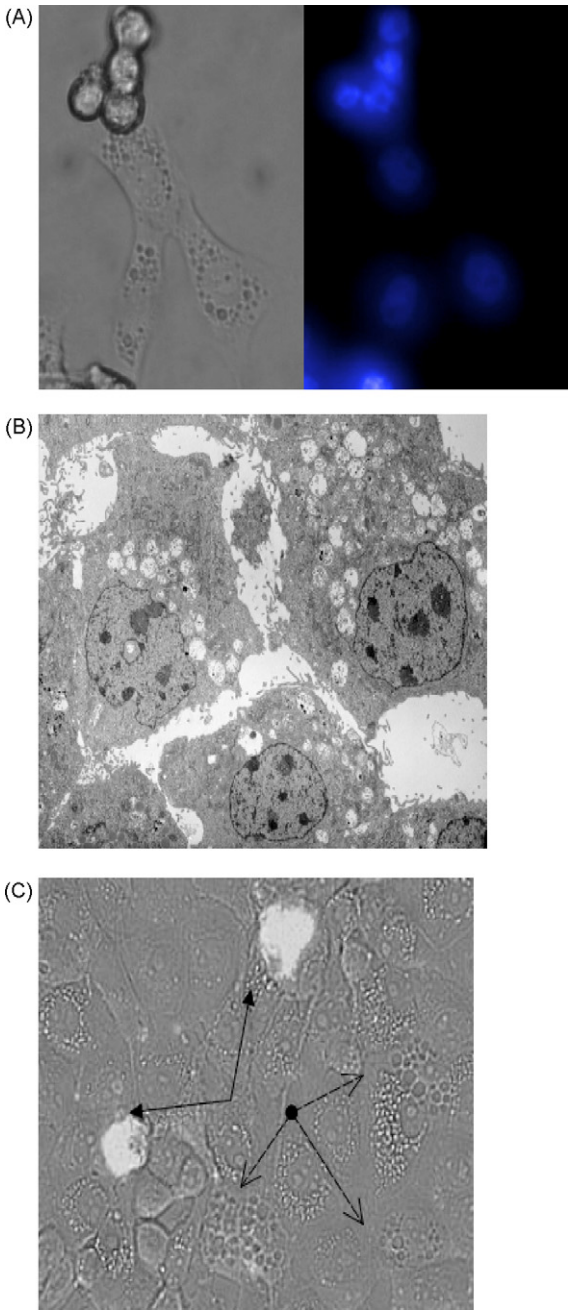

Fig. 6. Cytoplasmic vacuolization in cpBVDV-infected cells is not associated with apoptotic markers. (A) Microscopic analysis of Hoechst dye staining in cpBVDV-infected MDBK cells 48 h post-infection demonstrates uniformly low intensity stained nuclei in vacuolized cells and brightly stained nuclei in detached cells. Left panel correspond to light microscopy of representative cells and right represents fluorescent microscopy of the same cells. (B) Electron microscopy of infected MDBK cell (16 h post-infection) demonstrates the absence of chromatin condensation in nuclei of highly vacuolized cells. (C) Microscopic analysis of FLICA dye staining in cpBVDV-infected MDBK cells 24 h post-infection. Light microscopic and fluorescent microscopic images for FLICA staining were superimposed demonstrating no staining of vacuolized cells (dashed arrows) and brightly stained apoptotic cells (solid arrows, filled arrow heads).

to MDBK cells prior to and during viral infection improved cell viability from $6.7 \pm 2.2\%$ to $18.8 \pm 2.2\%$ (Fig. 5B), caspase inhibition had no effect on the appearance of vacuoles (Fig. 5A) in infected cells 24 h post-infection, suggesting that virus-induced cytoplasmic vacuolization is caspase-independent.

We further investigated whether apoptotic markers were localized to the infected cells with extensive cytoplasmic vacuolization. We demonstrated that at 48 h post-infection, the nuclei of cells, which were still attached with extensive vacuolization showed no evidence of bright staining with Hoechst 33324 and chromatin condensation (Fig. 6A). On the other hand, detached cells were labeled by the Hoechst dye, producing bright

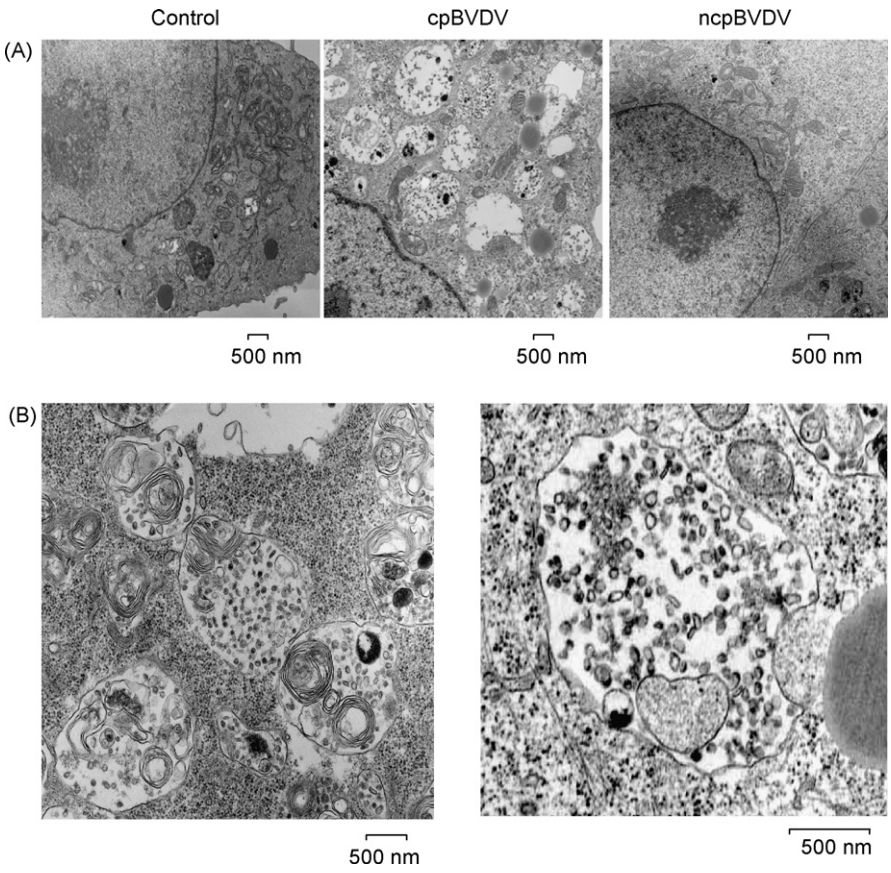

Fig. 7. (A) Electron micrographic analysis of representative control, ncpBVDV and cpBVDV-infected MDBK cell 24 h post-infection. Large vacuoles (V), encapsulated by single membranes and containing cellular debris, are found only in the cytoplasm of infected cells. Mitochondria and nuclei appear to be normal in infected cells. (B) Ultrastructural analysis of representative cytoplasmic vacuoles found in infected cells. Large encapsulated vacuoles were found to fuse with each other, forming larger vacuoles (left panel). Some of cytoplasmic autophagic vacuoles were found to be in a process of engulfing cytoplasmic material (as indicated by arrows) (right panel).

fluorescence, and nuclei in those cells were very poorly defined (Fig. 6A). To further characterize the apoptosis-vacuolization association on the ultrastructural level, we examined the nuclei of highly vacuolated cells at 16 h post-infection using electron microscopy. We found that none of the highly vacuolized cells had apoptotic bodies or condensed chromatin in their nuclei (Fig. 6B). Moreover, infected cells with extensive cytoplasmic vacuolization did not have FLICA staining, a marker for caspase activation (Fig. 6C).

Further examination of the cytoplasmic vacuoles observed after cpBVDV infection on ultrastructural level, demonstrated that the vacuoles are surrounded by a clearly defined single membrane and contain remains of organelles and cell debris (Fig. 7). The virus-induced vacuoles were larger than 500 nm in diameter, with an average of 10 ± 1 vacuoles per cell per thin section examined. Control cells had some cells with cytoplasmic vacuoles smaller than 100 nm in diameter, averaging 1–2 vacuoles per cell (Fig. 7A). Cells infected with noncytopathic BVDV had cytoplasmic vacuolization similar to control cells (Fig. 7A). In addition, we were able to identify vacuoles that can fuse with each other (Fig. 7B, left panel) and can engulf surrounding cytoplasm and organelles (Fig. 7B, right panel), which could be a pathway for the formation of enlarged vacuoles.

Interestingly, in all infected cells examined by electron microscopy, there were no signs of autophagosomes, i.e. dense vacuoles surrounded by a double membrane, suggesting that macroautophagy is unlikely to be responsible for cpBVDV-induced cytoplasmic vacuolization. To further rule out the involvement of macroautophagy in virus-induced cytoplasmic vacuolization, we demonstrated that wortmannin, an PI3-kinase and macroautophagy inhibitor, at concentrations between 0.1 and 10 μM had no effect on cytoplasmic vacuolization induced by cpBVDV at 24 h post-infection (Fig. 8A). Treatment of cells with wortmannin also had no effect on cell viability either in control cell or infected cells (Fig. 8B).

The presence of cytoplasmic and organelle debris in cpBVDV-induced vacuoles might be suggestive of lysosomal involvement. Thus, we investigated lysosomal involvement in cpBVDV-induced vacuolization using the lysosome-specific dye, LysoTracker Red. We found that cells with extensive vacuolization of cytoplasm demonstrated a partial loss of typical punctuated LysoTracker Red fluorescence staining compared to cells without vacuolization. Fig. 9, and it was found to be distributed throughout cytoplasm of infected cells. Interestingly, LysoTracker Red, which labels acidic cellular compartments including macroautophagy-associated autophagolyso-

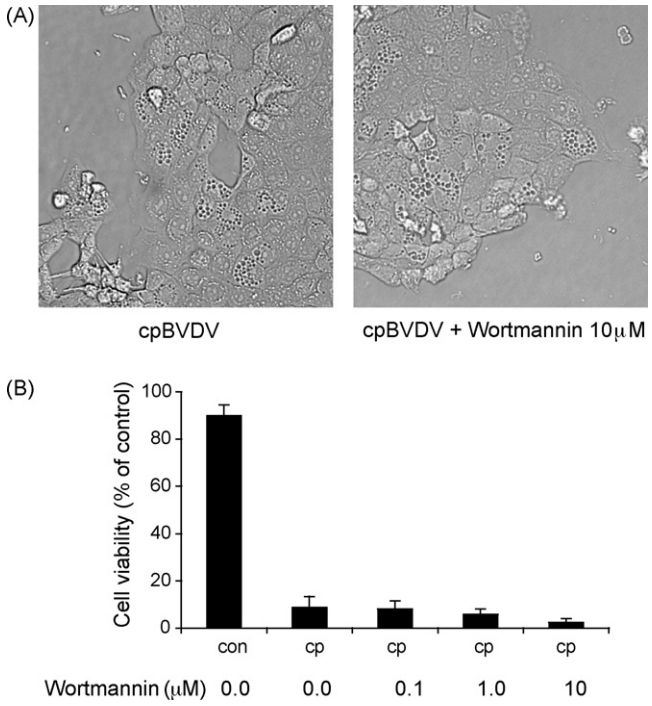

Fig. 8. Cytoplasmic vacuolization induced by cpBVDV is insensitive to treatment with wortmannin. (A) Light microscopy of infected MDBK cell (16 h post-infection) demonstrates that cpBVDV-induced cytoplasmic vacuolization is not affected by treatment with 10 μM wortmannin. (B) Wortmannin (0.1–10 μM) had no effect on decrease in cell viability mediated by cpBVDV infection.

somes, did not label cytoplasmic vacuoles in cpBVDV (Fig. 9).

4. Discussion

Cytoplasmic vacuolization is a commonly noted response in cells infected with the cytopathic biotype of BVDV. However, there are no detailed reports directly linking the vacuoles to the presence of virus in the infected cell. In this work, using a monoclonal antibody to viral protein, NS3, to identify BVDV-infected cells (Deregt et al., 2005), we demonstrated that NS3 can be easily detected in infected cells with cytoplasmic vacuolization, suggesting the virus induces vacuolization of infected MDBK cells. Interestingly, ncpBVDV does not produce any morphological changes in infected cells, and can actually block CPE when co-infected with cpBVDV (Bendfeldt et al., 2003; Yamane et al., 2005). Thus, vacuolization is unlikely to be important for viral replication. In support of this hypothesis, we demonstrated that NS3, which is required for viral replication (Gu et al., 2000), was identified throughout the cytoplasm of infected cells, but the lumen of vacuoles were free of this protein.

Extensive cytoplasmic vacuolization is thought to be associated with necrosis and necroapoptosis (Degterev et al., 2005; Kitanaka and Kuchino, 1999; Kroemer et al., 2005). Here we demonstrated that infected cells with extensive cellular vacuolization are impermeable to propidium iodide, suggesting virus-induced vacuolization does not alter plasma membrane integrity, a hallmark of necrosis (Kroemer et al., 2005). In addition, mitochondria in BVDV-infected cells appear to be normal, unlike mitochondrial abnormalities, such as swelling, that are observed during necrosis and necroptosis (Degterev et al., 2005). This also suggests that necrotic events are unlikely to be primary reasons for cytoplasmic vacuolization in infected cells.

To address the question of apoptosis versus cellular vacuolization during cpBVDV infection, we found that cellular vacuolization is a major early response to viral infection as compared to the late apoptotic response of chromatin condensation. In addition, cells with extensive cytoplasmic vacuolization have morphologically normal nuclei, which are not brightly stained with the Hoechst dye. These data are in agreement with our electron microscopy study demonstrating that highly vacuolized cells do not show evidence of apoptotic bodies or chromatin condensation. Although, in agreement with other publications (Grummer et al., 2002b; Jordan et al., 2002; Schweizer and Peterhans, 1999), caspase activation was also observed at 24 h post-infection, but cytochemical examination showed an absence of caspase activation in cells with extensive cytoplasmic vacuolization (Fig. 6C). These data suggest that caspase activa-

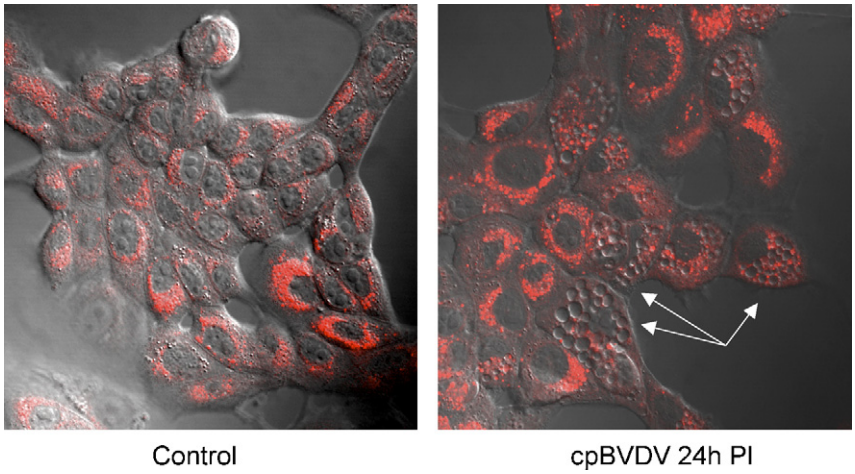

Fig. 9. Microscopic analysis of LysoTracker Red fluorescence in cpBVDV-infected MDBK cells, demonstrating bright fluorescence in morphologically normal cells and depletion of fluorescence in vacuolized cells (arrow).

tion is not involved in virus-induced cytoplasmic vacuolization responses.

A recent study of cells infected with the coronavirus mouse hepatitis virus (MHV), another cytoplasmic positive sense RNA virus, showed extensive vacuolization of the cytoplasm thought to be associated with autophagy (Prentice et al., 2004). This does not appear to be the case for BVDV. Three classes of autophagy have been described: macroautophagy, chaperone-mediated autophagy, and microautophagy. Macroautophagy and chaperone-mediated autophagy are normal cellular stress responses designed to remove and recycle misfolded proteins and damaged organelles (Cuervo, 2004; Shintani and Klionsky, 2004). Electron microscopy of macroautophagic responses reveals two subtypes of electron-dense macroautophagic vacuoles:autophagosomes and autophagolysosomes (Eskelinen, 2005; Lawrence and Brown, 1992) both of which are double membrane-bound structures. These macroautophagic structures are also labeled with LysoTracker Red which is easily detected by wide-field and confocal fluorescent microscopy (Moriyasu et al., 2003; Rideout et al., 2004). Pharmacologically, macroautophagy can be distinguished from the other types of autophagy by its sensitivity to wortmannin and other phosphoinositide 3-kinases (PI3-kinase) inhibitors (Finn et al., 2005; Petiot et al., 2000). The BVDV-induced vacuoles are single membrane structures not labeled with LysoTracker Red.

Recently, microtuble-associated protein lightchain 3 (LC3), a mammalian homolog of yeast Atg8, has been put forth as a specific marker to monitor macroautophagy. LC3 was found to be co-localized with LysoTracker-stained macroautophagic structures (Bampton et al., 2005). However, further work on LC3 and macroautophagy indicates that LC3 could be incorporated into protein aggregates independent of autophagy (Kuma et al., 2007). In addition, detection of macroautophagy-associated LC3 conversion (LC3 I to LC3 II) could be problematic because LC3 II tends to be much more sensitive to detection by immunoblotting than LC3 I (Mizushima and Yoshimori, 2007). We chose not to pursue LC3 staining for the above reason and because the EM morphological studies, LysoTracker staining, and insensitivity to wortmannin clearly demonstrated that virus-induced vacuolization is inconsistent with macroautophagy. Chaperone-mediated autophagy does not exhibit cytoplasmic vacuoles and can only be detected with specific probes (Kaushik and Cuervo, 2006; Kaushik et al., 2006). Microautophagy (Kunz et al., 2004; Muller et al., 2000; Sattler and Mayer, 2000) is defined as the sequestration of cytoplasmic components by direct invagination of lysosomal or vesicular membrane, followed by budding of engulfed small vesicular structures into the lumen of the autophagolysosomes containing cellular debris. This process is topologically equivalent to membrane invagination during multivesicular body formation and to the budding of enveloped viruses (Kunz et al., 2004). Functionally, microautophagy is associated with macroautophagy, thus, counterbalancing macroautophagy-mediated membrane influx, which is essential for resumption of cell growth (Dubouloz et al., 2005).

We did not find electron-dense double-membraned autophagosomes and autophagolysosomes, typical hallmarks of macroautophagy (Cuervo, 2004), suggesting that macroautophagy is unlikely to be involved in cellular response to BVDV. Furthermore, we determine that the PI-3 kinase inhibitor, wortmannin (0.1–10 μM), known to block macroautophagy even at 0.1 μM (Finn et al., 2005), had no effect on either cytoplasmic vacuolization or cell survival. These data would also suggest that vacuolization induced by BVDV is PI-3 kinase-independent. Furthermore, we demonstrated that the cytoplasmic vacuoles were not stained with LysoTracker Red. Thus, the absence of three out of four parameters for determination of macroautophagy suggests that BVDV-induced vacuolization is different from macroautophagy.

The ultrastructural morphological nature of BVDV-induced cytoplasmic vacuoles was examined by electron microscopy. We determined that the vacuoles in infected cells contain organelles' and cytoplasmic debris. Further examination of cytoplasmic vacuoles revealed that they are capable of fusing with each other and engulfing surrounding cytoplasmic components, suggesting that virus-induced vacuoles possess phagocytic properties. This morphological observation correlates well with extensive growth of vacuoles and disappearance of cytoplasm in infected cells, demonstrated at the level of light microscopy. This morphology is consistent with previously described microautophagy, where the cytoplasmic vacuoles seem to be the primary mechanism for sequestering cytoplasm and organelles in cells (Tuttle and Dunn, 1995; Tuttle et al., 1993; Veenhuis et al., 1983; Yokota et al., 1993). However, the phagocytic vacuolization response induced by the virus seems to be cytotoxic, which is different from postulated functional role of microautophagy for cell survival (Dubouloz et al., 2005). In addition, because microautophagy is thought to be in a close association with macroautophagy, the absence of BVDV-induced macroautophagy could also suggest the absence of virus-induced microautophagy. Therefore, cpBVDV-induced cytoplasmic phagocytic vacuolization appears to be morphologically similar to microautophagy, but functionally it is different from previously described macroautophagy, chaperon-mediated autophagy, and microautophagy.

Although not extensively covered by this study, it would be worthwhile to point out that LysoTracker Red staining throughout the cytoplasm of infected cells is indicative of lysosomal abnormality (Caruso et al., 2005). If lysomal dysfunction occurs, an appearance of lysosomal enzymes such as cathepsins and serine proteases in cytoplasm is likely to result in activation of number of caspase-dependent and caspase-independent pathways in addition to general cell lysis, as was initially described in serum-starved PC12 cells (Uchiyama, 2001). Interestingly, a significant proportion of viral NS3, produced during infection with cytopathic BVDV strains, was found to be associated with smooth endoplasmic reticulum (Zhang et al., 2003), known to be involved in the formation of lysosomes (Novikoff, 1976). Thus, it is possible that the stress induced by NS3 on smooth endoplasmic reticulum in cells infected with cytopathic strains of BVDV could be the cause of lysosomal abnormalities and induction of formation of cytoplasmic vacuoles with phagocytic properties.

In recent years, there has been much interest in the role of cellular structures in the replication of numerous viruses. Evidence has been presented to suggest that autophagy is induced

by viruses to provide intracellular compartments and scaffolds to assist the replication process (Novoa et al., 2005; Wileman, 2006). BVDV provides some unique insight into this area in that two biotypes of the virus exist, one that induces extensive vacuole formation (cpBVDV) and the other which does not (ncpBVDV). Both biotypes replicate equally well to produce infectious progeny, which indicates that the formation of vacuoles is irrelevant to virus replication. The autophagy-like response in this instance may be more related to a cellular defense mechanism of an innate or adaptive immune response (Deretic, 2005).

In conclusion, we demonstrate here that the autophagy-like cellular response is an early response to cpBVDV infection. This cellular response to the virus is different from apoptosis, necrosis, and recently described necroapoptosis. Virus-induced vacuoles possess phagocytic properties, responsible for digestion of cytoplasm and cytoplasmic components, suggesting that this form of vacuole-mediated autolysis could be named phagoptosis.

Acknowledgments

We thank Dr. Joel D. Pardee for the excellent and very useful discussions.

This work was supported by NIH/NIDA grant, K01 DAO18262, and a seed grant from Cornell University.

References

Bampton, E.T., Goemans, C.G., Niranjan, D., Mizushima, N., Tolkovsky, A.M., 2005. The dynamics of autophagy visualized in live cells: from autophagosome formation to fusion with endo/lysosomes. Autophagy 1, 23–36.

Bendfeldt, S., Grummer, B., Greiser-Wilke, I., 2003. No caspase activation but overexpression of Bcl-2 in bovine cells infected with noncytopathic bovine virus diarrhoea virus. Vet. Microbiol. 96, 313–326.

Bielefeldt Ohmann, H., Bloch, B., 1982. Electron microscopic studies of bovine viral diarrhea virus in tissues of diseased calves and in cell cultures. Arch. Virol. 71, 57–74.

Bolin, S.R., McClurkin, A.W., Cutlip, R.C., Coria, M.F., 1985. Severe clinical disease induced in cattle persistently infected with noncytopathic bovine viral diarrhea virus by superinfection with cytopathic bovine viral diarrhea virus. Am. J. Vet. Res. 46, 573–576.

Brownlie, J., 1991. The pathways for bovine virus diarrhoea virus biotypes in the pathogenesis of disease. Arch. Virol. Suppl. 3, 79–96.

Brownlie, J., Clarke, M.C., Howard, C.J., 1984. Experimental production of fatal mucosal disease in cattle. Vet. Rec. 114, 535–536.

Caruso, J.A., Mathieu, P.A., Reiners Jr., J.J., 2005. Sphingomyelins suppress the targeted disruption of lysosomes/endosomes by the photosensitizer NPe6 during photodynamic therapy. Biochem. J. 392, 325–334.

Collett, M.S., Anderson, D.K., Retzel, E., 1988. Comparisons of the pestivirus bovine viral diarrhoea virus with members of the flaviviridae. J. Gen. Virol. 69 (Pt 10), 2637–2643.

Cuervo, A.M., 2004. Autophagy: many paths to the same end. Mol. Cell. Biochem. 263, 55–72.

Degterev, A., Huang, Z., Boyce, M., Li, Y., Jagtap, P., Mizushima, N., Cuny, G.D., Mitchison, T.J., Moskowitz, M.A., Yuan, J., 2005. Chemical inhibitor of nonapoptotic cell death with therapeutic potential for ischemic brain injury. Nat. Chem. Biol. 1, 112–119.

Deregt, D., Dubovi, E.J., Jolley, M.E., Nguyen, P., Burton, K.M., Gilbert, S.A., 2005. Mapping of two antigenic domains on the NS3 protein of the pestivirus bovine viral diarrhea virus. Vet. Microbiol. 108, 13–22.

Deretic, V., 2005. Autophagy in innate and adaptive immunity. Trends Immunol. 26, 523–528.

Dubouloz, F., Deloche, O., Wanke, V., Cameroni, E., De Virgilio, C., 2005. The TOR and EGO protein complexes orchestrate microautophagy in yeast. Mol. Cell 19, 15–26.

Eskelinen, E.L., 2005. Maturation of autophagic vacuoles in mammalian cells. Autophagy 1, 1–10.

Finn, P.F., Mesires, N.T., Vine, M., Dice, J.F., 2005. Effects of small molecules on chaperone-mediated autophagy. Autophagy 1, 141–145.

Grummer, B., Moennig, V., Greiser-Wilke, I., 1998. Cytopathogenic bovine viral diarrhea viruses induce apoptosis in bovine cell cultures. Dtsch. Tierarztl. Wochenschr. 105, 29–31.

Grummer, B., Bendfeldt, S., Greiser-Wilke, I., 2002a. Apoptosis inhibitors delay the cytopathic effect of bovine viral diarrhoea virus (BVDV). J. Vet. Med. B Infect Dis. Vet. Public Health 49, 298–303.

Grummer, B., Bendfeldt, S., Wagner, B., Greiser-Wilke, I., 2002b. Induction of the intrinsic apoptotic pathway in cells infected with cytopathic bovine virus diarrhoea virus. Virus Res. 90, 143–153.

Gu, B., Liu, C., Lin-Goerke, J., Maley, D.R., Gutshall, L.L., Feltenberger, C.A., Del Vecchio, A.M., 2000. The RNA helicase and nucleotide triphosphatase activities of the bovine viral diarrhea virus NS3 protein are essential for viral replication. J. Virol. 74, 1794–1800.

Jordan, R., Wang, L., Graczyk, T.M., Block, T.M., Romano, P.R., 2002. Replication of a cytopathic strain of bovine viral diarrhea virus activates PERK and induces endoplasmic reticulum stress-mediated apoptosis of MDBK cells. J. Virol. 76, 9588–9599.

Kaushik, S., Cuervo, A.M., 2006. Autophagy as a cell-repair mechanism: activation of chaperone-mediated autophagy during oxidative stress. Mol. Aspects Med. 27, 444–454.

Kaushik, S., Massey, A.C., Cuervo, A.M., 2006. Lysosome membrane lipid microdomains: novel regulators of chaperone-mediated autophagy. Embo. J. 25, 3921–3933.

Kitanaka, C., Kuchino, Y., 1999. Caspase-independent programmed cell death with necrotic morphology. Cell Death Differ. 6, 508–515.

Kroemer, G., El-Deiry, W.S., Golstein, P., Peter, M.E., Vaux, D., Vandenabeele, P., Zhivotovsky, B., Blagosklonny, M.V., Malorni, W., Knight, R.A., Piacentini, M., Nagata, S., Melino, G., 2005. Classification of cell death: recommendations of the nomenclature committee on cell death. Cell Death Differ. 12 (Suppl 2), 1463–1467.

Kuma, A., Matsui, M., Mizushima, N., 2007. LC3, an autophagosome marker, can be incorporated into protein aggregates independent of autophagy: caution in the interpretation of LC3 localization. Autophagy 3, 323–328.

Kunz, J.B., Schwarz, H., Mayer, A., 2004. Determination of four sequential stages during microautophagy in vitro. J. Biol. Chem. 279, 9987–9996.

Lawrence, B.P., Brown, W.J., 1992. Autophagic vacuoles rapidly fuse with pre-existing lysosomes in cultured hepatocytes. J. Cell Sci. 102 (Pt 3), 515–526.

Mazzio, E.A., Soliman, K.F., 2004. Glioma cell antioxidant capacity relative to reactive oxygen species produced by dopamine. J. Appl. Toxicol. 24, 99–106.

Mizushima, N., Yoshimori, T., 2007. How to interpret LC3 immunoblotting. Autophagy, 3.

Moriyasu, Y., Hattori, M., Jauh, G.Y., Rogers, J.C., 2003. Alpha tonoplast intrinsic protein is specifically associated with vacuole membrane involved in an autophagic process. Plant Cell Physiol. 44, 795–802.

Muller, O., Sattler, T., Flotenmeyer, M., Schwarz, H., Plattner, H., Mayer, A., 2000. Autophagic tubes: vacuolar invaginations involved in lateral membrane sorting and inverse vesicle budding. J. Cell Biol. 151, 519–528.

Novikoff, A.B., 1976. The endoplasmic reticulum: a cytochemist's view (a review). Proc. Natl. Acad. Sci. USA 73, 2781–2787.

Novoa, R.R., Calderita, G., Arranz, R., Fontana, J., Granzow, H., Risco, C., 2005. Virus factories: associations of cell organelles for viral replication and morphogenesis. Biol. Cell 97, 147–172.

Petiot, A., Ogier-Denis, E., Blommaart, E.F., Meijer, A.J., Codogno, P., 2000. Distinct classes of phosphatidylinositol 3'-kinases are involved in signaling pathways that control macroautophagy in HT-29 cells. J. Biol. Chem. 275, 992–998.

Prentice, E., Jerome, W.G., Yoshimori, T., Mizushima, N., Denison, M.R., 2004. Coronavirus replication complex formation utilizes components of cellular autophagy. J. Biol. Chem. 279, 10136–10141.

Rideout, H.J., Lang-Rollin, I., Stefanis, L., 2004. Involvement of macroautophagy in the dissolution of neuronal inclusions. Int. J. Biochem. Cell. Biol. 36, 2551–2562.

Sattler, T., Mayer, A., 2000. Cell-free reconstitution of microautophagic vacuole invagination and vesicle formation. J. Cell Biol. 151, 529–538.

Schweizer, M., Peterhans, E., 1999. Oxidative stress in cells infected with bovine viral diarrhoea virus: a crucial step in the induction of apoptosis. J. Gen. Virol. 80 (Pt 5), 1147–1155.

Shintani, T., Klionsky, D.J., 2004. Autophagy in health and disease: a double-edged sword. Science 306, 990–995.

Tuttle, D.L., Dunn Jr., W.A., 1995. Divergent modes of autophagy in the methylotrophic yeast Pichia pastoris. J. Cell Sci. 108 (Pt 1), 25–35.

Tuttle, D.L., Lewin, A.S., Dunn Jr., W.A., 1993. Selective autophagy of peroxisomes in methylotrophic yeasts. Eur. J. Cell Biol. 60, 283–290.

Uchiyama, Y., 2001. Autophagic cell death and its execution by lysosomal cathepsins. Arch. Histol. Cytol. 64, 233–246.

Veenhuis, M., Douma, A., Harder, W., Osumi, M., 1983. Degradation and turnover of peroxisomes in the yeast Hansenula polymorpha induced by selective inactivation of peroxisomal enzymes. Arch. Microbiol. 134, 193–203.

Wileman, T., 2006. Aggresomes and autophagy generate sites for virus replication. Science 312, 875–878.

Yamane, D., Nagai, M., Ogawa, Y., Tohya, Y., Akashi, H., 2005. Enhancement of apoptosis via an extrinsic factor, TNF-alpha, in cells infected with cytopathic bovine viral diarrhea virus. Microbes. Infect. 7, 1482–1491.

Yokota, S., Himeno, M., Roth, J., Brada, D., Kato, K., 1993. Formation of autophagosomes during degradation of excess peroxisomes induced by di-(2-ethylhexyl)phthalate treatment. II. Immunocytochemical analysis of early and late autophagosomes. Eur. J. Cell Biol. 62, 372–383.

Zhang, G., Aldridge, S., Clarke, M.C., McCauley, J.W., 1996. Cell death induced by cytopathic bovine viral diarrhoea virus is mediated by apoptosis. J. Gen. Virol. 77 (Pt 8), 1677–1681.

Zhang, G., Flick-Smith, H., McCauley, J.W., 2003. Differences in membrane association and sub-cellular distribution between NS2-3 and NS3 of bovine viral diarrhoea virus. Virus Res. 97, 89–102.